Journal of Crystal Growth 474 (2017) 160–165

Contents lists available at ScienceDirect

Journal of Crystal Growth

journal homepage: www.elsevier.com/locate/jcrysgro

Multi-phase-field study of the effects of anisotropic grain-boundary properties on polycrystalline grain growth

Eisuke Miyoshi[a], Tomohiro Takaki[b,*]

[a] Department of Mechanical and System Engineering, Kyoto Institute of Technology, Matsugasaki, Sakyo, Kyoto 606-8585, Japan
[b] Faculty of Mechanical Engineering, Kyoto Institute of Technology, Matsugasaki, Sakyo, Kyoto 606-8585, Japan

ARTICLE INFO

Communicated by Dr Francois Dupret

Keywords:
A1. Computer simulation
A1. Growth models
A1. Interface
B1. Polycrystalline growth

ABSTRACT

Numerical studies of the effects of anisotropic (misorientation-dependent) grain-boundary energy and mobility on polycrystalline grain growth have been carried out for decades. However, conclusive knowledge has yet to be obtained even for the simplest two-dimensional case, which is mainly due to limitations in the computational accuracy of the grain-growth models and computer resources that have been employed to date. Our study attempts to address these problems by utilizing a higher-order multi-phase-field (MPF) model, which was developed to accurately simulate grain growth with anisotropic grain-boundary properties. In addition, we also employ general-purpose computing on graphics processing units to accelerate MPF grain-growth simulations. Through a series of simulations of anisotropic grain growth, we succeeded in confirming that both the anisotropies in grain-boundary energy and mobility affect the morphology formed during grain growth. On the other hand, we found the grain growth kinetics in anisotropic systems to follow parabolic law similar to isotropic growth, but only after an initial transient period.

1. Introduction

During heat treatment of polycrystalline materials, grain growth is one of the most important metallurgical phenomena, because it enables the microstructure of the materials to be controlled to produce materials with superior mechanical and physical properties. In general, the fundamental process underlying grain growth is the migration of grain boundaries, and thus, the grain-growth behavior is largely affected by the grain-boundary properties [1]: energy, γ, and mobility, M. These properties are not isotropic, with their variation depending primarily on the misorientation angle between neighboring grains [1–4]. However, it is difficult to incorporate these anisotropic properties directly into analytical theories [5–7]. Therefore, the effects of the anisotropic properties on grain growth have frequently been investigated systematically by performing numerical simulations [2,8–24].

Essentially, a study of the anisotropy effects involves studying two-dimensional anisotropic grain growth in a randomly textured system with two-dimensional crystal lattices. In this regard, several studies have been conducted using meso-scale grain-growth models: the Monte-Carlo model [9,10,19,22,24], the vertex model [2,21], and the phase-field model [16,22]. However, even for the simple two-dimensional case, there has not been consensus on the correlations between grain-boundary properties and grain-growth behavior. For instance, whereas Frost et al. [9], Yu and Essche [24], Saito and Enomoto [19], and Moelans et al. [16] suggested that the growth kinetics with the energy anisotropy follows the well-known parabolic law [2] similar to the isotropic case, Grest et al. [10] and Upmanyu et al. [22] reported significant deviations from the parabolic law. Moreover, in contrast to the vertex simulations conducted by Humphreys [2] that showed clear contributions of the mobility anisotropy on grain growth, the Monte-Carlo and phase-field study by Upmanyu et al. [22] concluded that the anisotropy in mobility has no impact. These discrepancies could be attributable to some limitations of the previous simulations [25]: a considerable amount of noise and lattice anisotropy in Monte-Carlo simulations, grain coalescence resulting from a limited number of grain orientations, or the use of a limited number of grains in the computation system, all of which prevent reliable statistics of grain growth from being obtained.

Lately, the multi-phase-field (MPF) model reported by Steinbach et al. [26,27] has been widely employed as a powerful tool for simulating several thermodynamic phenomena including grain growth. This model can treat curvature-driven boundary migration with high accuracy while taking realistic material parameters into account. Moreover, it is easy to introduce the active parameter tracking algorithm [28–31], which was proposed by three research groups [25,32,33] independently, in this model; this increases the computa-

* Corresponding author.
E-mail address: takaki@kit.ac.jp (T. Takaki).

http://dx.doi.org/10.1016/j.jcrysgro.2016.11.097

Available online 24 November 2016

tion speed significantly and enables large numbers of orientations (or grains) to be processed. However, the original MPF model does not allow for the introduction of the anisotropic grain-boundary properties for wide-ranging misorientation angles. This is because the model becomes numerically unstable in the case of calculations in which the energies or mobilities of the grain boundaries adjoining a triple junction exhibit large differences. Garcke et al. [34,35] and Hirouchi et al. [36] have attempted to overcome this issue by proposing modified models, which are referred to as higher-order MPF models, that contain higher-order terms to represent the free energy of the triple junction. However, a suitable method for modeling the simulation parameters used in such models has not been established. Therefore, the authors of this paper constructed a novel higher-order MPF model and confirmed its validity for two-dimensional grain-growth simulations using anisotropic grain-boundary properties [37].

The purpose of this paper is to present statistically and numerically reliable knowledge on two-dimensional anisotropic grain growth. To this effect, the higher-order MPF model that was proposed in our previous study [37] was used to perform anisotropic grain-growth simulations for two-dimensional systems including large numbers of grains. The MPF simulations were accelerated by employing graphics processing units (GPUs) [38–43]. The simulations enabled a detailed investigation of the individual and coupled effects of the misorientation-dependent grain-boundary energy and mobility on grain growth.

2. Computational method

2.1. Higher-order MPF model

This section presents a description of the higher-order MPF model [37] that was employed for the grain-growth simulations. The model represents a polycrystalline system including N grains by phase-field variables ϕ_α ($\alpha = 1, 2, \ldots, N$), which take a value of 1 in the αth grain, 0 in the other grains, and $0 < \phi_\alpha < 1$ at the grain boundaries. These ϕ_α are not independent and must satisfy

$$\sum_{\alpha=1}^{N} \phi_\alpha = 1. \tag{1}$$

The free-energy functional of the system is assumed as follows using ϕ_α :

$$F = \int_V \sum_{\alpha=1}^{N} \sum_{\beta=\alpha+1}^{N} \left(W_{\alpha\beta}\phi_\alpha\phi_\beta + \sum_{\chi=\beta+1}^{N} W_{\alpha\beta\chi}\phi_\alpha\phi_\beta\phi_\chi - \frac{a_{\alpha\beta}^2}{2}\nabla\phi_\alpha\cdot\nabla\phi_\beta \right) \mathrm{d}V, \tag{2}$$

where $W_{\alpha\beta}$ and $a_{\alpha\beta}$ are the barrier height and the gradient coefficient of the boundary between the αth and βth grains, respectively. The second term on the right-hand side in Eq. (2) is the higher-order term representing the additional free energy of the triple junctions, which is not accounted for in the original MPF model by Steinbach et al. [26,27]. The higher-order term is employed to suppress the formation of an extra phase at the grain boundaries around the junctions. The coefficient $W_{\alpha\beta\chi}$ is the barrier height of the junction, and is modeled as

$$W_{\alpha\beta\chi} = \begin{cases} k\left(W_{\max} - \frac{W_{\mathrm{median}} + W_{\min}}{2}\right) & \text{for} 2W_{\mathrm{median}} \le W_{\max} + W_{\min}, \\ 0 & \text{for} 2W_{\mathrm{median}} > W_{\max} + W_{\min}, \end{cases} \tag{3}$$

where $W_{\max}$, W_{median}, and $W_{\min}$ are the maximum, median, and minimum barrier heights, respectively, for the grain boundaries adjoining the triple junction, and k=4 is a constant. The time-evolution equation of the phase field ϕ_i ($i = 1, 2, \ldots, n$) satisfying Eq. (1) is given for each spatial point by

$$\frac{\partial\phi_i}{\partial t} = -\frac{2}{n} \sum_{j=1}^{n} M_{ij}^{\phi} \left(\frac{\delta F}{\delta\phi_i} - \frac{\delta F}{\delta\phi_j} \right), \tag{4}$$

where n is the number of non-zero phase fields at a point and M_{ij}^{ϕ} is the phase-field mobility of the boundary between the i^{th} and j^{th} grains. The functional derivative of Eq. (2) can be calculated as

$$\frac{\delta F}{\delta\phi_i} = \sum_{k=1}^{n} \left(W_{ik}\phi_k + \sum_{l=1}^{n} W_{ikl}\phi_k\phi_l + \frac{a_{ik}^2}{2}\nabla^2\phi_k \right). \tag{5}$$

Finally, the time-evolution equation reduces to

$$\frac{\partial\phi_i}{\partial t} = -\frac{2}{n} \sum_{j=1}^{n} M_{ij}^{\phi} \left[\sum_{k=1}^{n} \left\{ (W_{ik} - W_{jk})\phi_k + \sum_{l=1}^{n} (W_{ikl} - W_{jkl})\phi_k \phi_l + \frac{1}{2}(a_{ik}^2 - a_{jk}^2)\nabla^2\phi_k \right\} \right]. \tag{6}$$

W_{ij}, a_{ij}, and M_{ij}^{ϕ} can be related to the thickness (δ), energy (γ_{ij}), and mobility (M_{ij}) of the boundary through the following equations:

$$W_{ij} = \frac{4\gamma_{ij}}{\delta}, \quad a_{ij} = \frac{2}{\pi}\sqrt{2\delta\gamma_{ij}}, \quad M_{ij}^{\phi} = \frac{\pi^2}{8\delta} M_{ij}. \tag{7}$$

Here, we introduce anisotropic mobility with a high degree of accuracy by modifying the definition of M_{ij}^{ϕ} in the triple junctions (n =3) as follows [37]:

$$\left.\begin{aligned} M_{ij}^{\phi} = M_{jk}^{\phi} = M_{ki}^{\phi} = \tfrac{\pi^2}{8\delta} M_{ijk} \\ M_{ijk} = M_{ij}\omega_{ij} + M_{jk}\omega_{jk} + M_{ki}\omega_{ki} \end{aligned}\right\} \quad \text{only for } n = 3, \tag{8}$$

where M_{ijk} is the triple-junction mobility and ω_{ij} is the weight function defined as follows using a constant m =10 and the average of the boundary mobilities $M_{\mathrm{ave}} = (M_{ij} + M_{jk} + M_{ki})/3$:

$$\omega_{ij} = \frac{1}{2}\left(1 - \frac{|M_{ij} - M_{\mathrm{ave}}|^m}{|M_{ij} - M_{\mathrm{ave}}|^m + |M_{jk} - M_{\mathrm{ave}}|^m + |M_{ki} - M_{\mathrm{ave}}|^m} \right). \tag{9}$$

2.2. Computational system and conditions

Fig. 1 exhibits the model we employed for simulating two-dimensional anisotropic grain growth. The domain was divided into a grid of 2400×2400 square regular cells with a size of Δx=1 μm. The system consisted of 16,000 grains that were under periodic boundary conditions in the x- and y-directions. The initial grain structure with a random shape was constructed through a normal grain-growth simulation from randomly distributed nuclei. The grain-boundary thickness, δ, and time step, Δt, were set to δ=6Δx=6 μm and Δt=0.1 s, respectively. The computations were performed for a period of 10,000 s (i.e.,

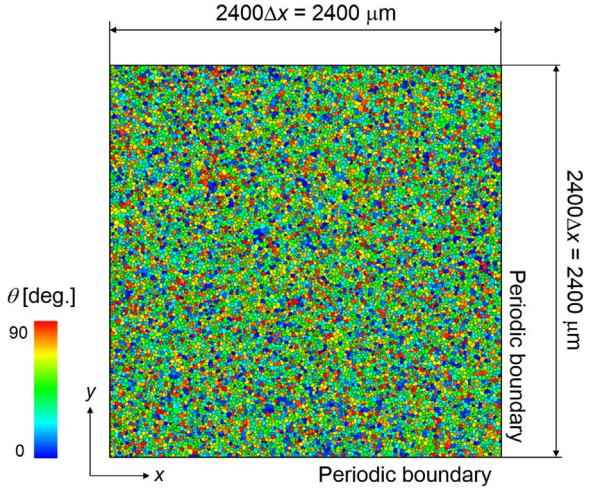

Fig. 1. Polycrystalline system used for the simulation of anisotropic grain growth. The initial structure is created through a normal grain-growth simulation.

100,000 steps). Assuming a two-dimensional crystal structure with a cubic symmetry, crystal orientations, θ, were randomly assigned to each grain within the range $0° \le \theta \le 90°$. The misorientation ($\Delta\theta_{ij}$) between grains i and j was determined as

$$\Delta\theta_{ij} = \min(|\theta_i - \theta_j|,\ 90 - |\theta_i - \theta_j|). \tag{10}$$

The misorientation-dependent grain-boundary energy, $\gamma_{ij}(\Delta\theta_{ij})$, and mobility, $M_{ij}(\Delta\theta_{ij})$, were expressed using the classical Read-Shockley (RS) model [44] and the sigmoidal model proposed by Humphreys [45], respectively as follows:

$$\gamma_{ij}(\Delta\theta_{ij}) = \begin{cases} \gamma_m \frac{\Delta\theta_{ij}}{\Delta\theta_m}\left\{1 - \ln\left(\frac{\Delta\theta_{ij}}{\Delta\theta_m}\right)\right\} & \text{for} \quad \Delta\theta_{ij} < \Delta\theta_m, \\ \gamma_m & \text{for} \quad \Delta\theta_{ij} \ge \Delta\theta_m, \end{cases} \tag{11}$$

$$M(\Delta\theta_{ij}) = \begin{cases} M_m\left[1 - \exp\left\{-5\left(-\frac{\Delta\theta_{ij}}{\Delta\theta_m}\right)^4\right\}\right] & \text{for} \quad \Delta\theta_{ij} < \Delta\theta_m, \\ M_m & \text{for} \quad \Delta\theta_{ij} \ge \Delta\theta_m, \end{cases} \tag{12}$$

where γ_m =1 J/m^2, M_m =1×10^{-12} m^4/(J·s), and $\Delta\theta_m$ =15° are the energy, mobility, and minimum misorientation of the high-angle grain boundaries, respectively. Note that when the anisotropic properties are introduced using Eqs. (11) and (12), the higher-order MPF model exhibits sufficient accuracy in the range of misorientation angles $\Delta\theta \ge 3°$[37]. Therefore, to obtain numerically reliable results, we maintained the values of γ and M as γ (3°) and M (3°) for those boundaries with $\Delta\theta < 3°$.

Using the above described conditions and the higher-order MPF model, grain-growth simulations were conducted for the following cases: (1) both γ and M are isotropic ($\gamma = \gamma_m$, $M = M_m$), (2) γ alone anisotropic ($\gamma = \gamma(\Delta\theta)$, $M = M_m$), (3) M alone anisotropic ($\gamma = \gamma_m$, $M = M(\Delta\theta)$), and (4) both γ and M anisotropic ($\gamma = \gamma(\Delta\theta)$, $M = M(\Delta\theta)$). Statistical reliability was guaranteed for each of these cases by obtaining numeric data points as the average of five simulation runs for different initial structures. Here, we developed our own CUDA C code to ensure the effective simulation of MPF grain growth by single-GPU (NVIDIA TESLA K20) computation; this was found to improve the computation speed by a factor of 10 compared to that of single-core computation on a CPU (Intel Xeon E5-2697).

3. Results and discussion

3.1. Morphological aspects of anisotropic systems

On the basis of the simulation results, we discuss the effects of the grain-boundary properties on the morphology formed during grain growth. Fig. 2 shows the simulated microstructures at t=10,000 s obtained for the above-mentioned four conditions of grain-boundary properties starting from the initial structure shown in Fig. 1. In Fig. 2, high-angle grain boundaries with misorientation angles $\Delta\theta \ge 15°$ are indicated by red lines, whereas the blue lines represent low-angle boundaries with line intensity proportional to $\Delta\theta$. In addition, the distribution of boundary misorientations and grain diameters, D, at the time, i.e., after 10,000 s, is shown in Fig. 3. The average of five replicate computations is plotted with error bars. Here, D is normalized with respect to the average grain diameter, D_{ave}. The D value of an individual grain, i, was estimated as

$$D_i = 2\sqrt{\frac{A_i}{\pi}}, \tag{13}$$

where A_i is the area of the grain i, which can be calculated as follows by integrating the corresponding phase field:

$$A_i = \int_s \phi_i dS. \tag{14}$$

Fig. 3 indicates that the grain distribution is statistically stable with small errors. The results shown in Figs. 2(a) and 3(a), with isotropic $\gamma = \gamma_m$ and $M = M_m$, enabled us to confirm a fully random texture, as expected. By contrast, the results in Figs. 2(b) and 3(a), with $\gamma = \gamma_m(\Delta\theta)$ and $M = M_m$, show that anisotropy only in the boundary energy leads to an increase in the fraction of low-angle (i.e., low-energy) boundaries; this is because low-angle boundaries are preferable for the reduction of the total free energy of the system. In this case, as shown in Fig. 3(b), the distribution in the size of the grains is similar to that of the isotropic systems. As shown in Figs. 2(c) and 3(a) with $\gamma = \gamma_m$ and $M = M_m(\Delta\theta)$, anisotropic mobility also increases the fraction of low-angle (i.e. low-mobility) boundaries. When the anisotropic mobility is expressed as Eq. (12), low-angle boundaries with $\Delta\theta < 6°$ take mobility values lower than those of high-angle boundaries by an order of magnitude, and these almost immobile boundaries remain for a long period. Moreover, Fig. 3(b) indicates that anisotropic mobility results in a slightly broader grain-size distribution than isotropic mobility. Fig. 2(d), for $\gamma = \gamma_m(\Delta\theta)$ and $M = M_m(\Delta\theta)$, clearly shows that the system incorporating both of the anisotropic properties displays a notably characteristic microstructure; the high-angle boundaries form their own grain-boundary network, within which the low-energy boundaries form sub-networks similar to a subgrain structure. In this case, as shown in Fig. 3, a significant increase in the prevalence of low-angle boundaries occurs, and the grain-size distribution becomes biased towards a small size. It should be noted that the formation of subgrain-like structures within a high-angle grain network has been reported in the form of a phase-field study performed by Moelans et al. [16], in which the anisotropy of boundary energy alone was introduced. However, in our simulation, which takes both the anisotropy of energy and mobility into account, this phenomenon is much more clearly recognizable compared to Fig. 2(b). This is probably a consequence of the combined effect of the anisotropic energy and mobility, besides the size of the system that was employed (5.5 times larger than that used in Ref. [16]).

The results summarized above enabled us to conclude that the anisotropy in both the boundary energy and mobility can affect the morphological characteristics of the microstructure formed through grain growth, especially when these two effects are coupled.

3.2. Kinetics of anisotropic grain growth

This section presents an examination of the kinetics of anisotropic grain growth. Firstly, let us consider the mean field theory of ideal grain growth by Burke and Turnbull [5]. According to their theory, the rate at which the average grain diameter, D_{ave}, changes is expressed as

$$\frac{dD_{ave}}{dt} = M_{ave}\frac{4\alpha\gamma_{ave}}{D_{ave}}, \tag{15}$$

where α is a geometric constant, and γ_{ave} and M_{ave} are the average energy and mobility of the grain boundaries, respectively. By integrating Eq. (15) with respect to time, the well-known parabolic growth law can be obtained as follows:

$$D_{ave}^n(t) - D_{ave}^n(t_0) = k(t - t_0), \tag{16}$$

where t_0 is an arbitrary initial time, n =2, and k=8$\alpha\gamma_{ave}M_{ave}$. The exponent n is commonly known as the grain-growth exponent. Note that the deformation of Eqs. (15) to (16) is impossible in cases where γ_{ave} or M_{ave} are time dependent. If Eq. (16) is adapted to such cases, the exponent n deviates from 2, typically being larger [1,2,12]. With this in mind, we calculated the temporal variations of the average misorientation ($\Delta\theta_{ave}$), energy, and mobility of the grain boundaries for isotropic and anisotropic systems. The results are shown in Fig. 4. Fig. 4(a) shows that $\Delta\theta_{ave}$ remains constant during isotropic growth ($\gamma = \gamma_m$, $M = M_m$). Moreover, even in anisotropic systems, the $\Delta\theta_{ave}$ values converge with time and become almost time independent. This implies that the distribution of misorientation angles reaches a steady

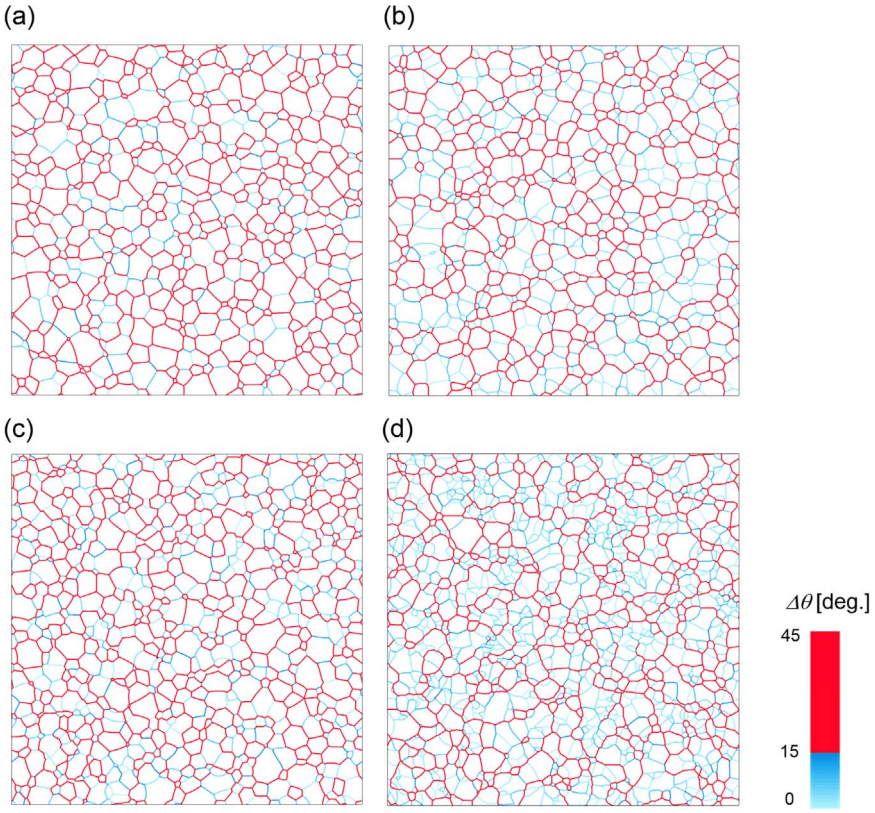

Fig. 2. Evolved microstructures obtained for different conditions of grain-boundary properties at simulation time t=10,000 s: (a) both γ and M are isotropic (γ= γ_m, M = M_m), (b) γ alone anisotropic (γ= γ ($\Delta\theta$), M = M_m), (c) M alone anisotropic (γ= γ_m, M = M ($\Delta\theta$)), and (d) both γ and M anisotropic (γ= γ ($\Delta\theta$), M = M ($\Delta\theta$)). The initial structure is that shown in Fig. 1. High-angle grain boundaries with misorientation angles $\Delta\theta \geq 15°$ are indicated by red lines, whereas the blue lines represent low-angle boundaries with line intensity proportional to $\Delta\theta$.

state, owing to the balance achieved between the possibilities to form and sweep a low-angle boundary. Consequently, as shown in Fig. 4(b) and (c), γ_{ave} and M_{ave}, which are determined by the misorientation distribution, also become constant. These results indicate that both anisotropic and isotropic growth are expected to follow Eq. (16) with n =2. We confirmed this by extracting the n values for the simulation results. Fig. 5 shows the temporal variations in the average grain diameter, D_{ave}, obtained for the four different conditions of grain-boundary properties. The grain-growth exponent is calculated by fitting the data plots to a curve using Eq. (16). For comparison, data fitting is carried out for two different simulation periods: 200≤ t [s] ≤3000 and 3000≤ t [s] ≤10,000, where, from Fig. 4, we can see almost constant $\Delta\theta_{ave}$, γ_{ave}, and M_{ave} after t=3000 s. The obtained values are shown in Table 1, in which the n values for the isotropic growth are 2.00 and 1.99; these are almost independent of time, and exhibit an excellent agreement with the theory. On the other hand, in the initial stages of the anisotropic growth simulations, the n values are larger than 2, indicating that the growth rate of the average grain size decreases more rapidly than in the isotropic case. However, as expected, the n values for the anisotropic cases all approach 2 in the later stages of the simulation.

On the basis of the above-mentioned results, we can conclude that, after a transient period (t=3000 s in the present simulations), the kinetics of anisotropic grain growth behaves according to the parabolic law similar to isotropic growth. This strongly suggests that the deviations from parabolic law observed in previous studies [10,22] may have resulted from the small number of grains, short simulation time, or insufficient accuracy of the particular grain-growth model that was employed.

4. Conclusions

This study investigated the effects of the misorientation-dependent grain-boundary energy and mobility on polycrystalline grain growth

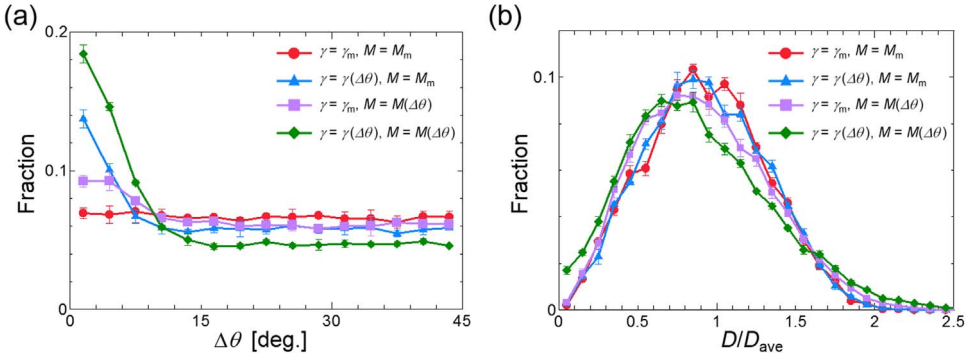

Fig. 3. Distributions of (a) $\Delta\theta$ and (b) D/D_{ave} obtained for different conditions of grain-boundary properties at simulation time t=10,000 s.

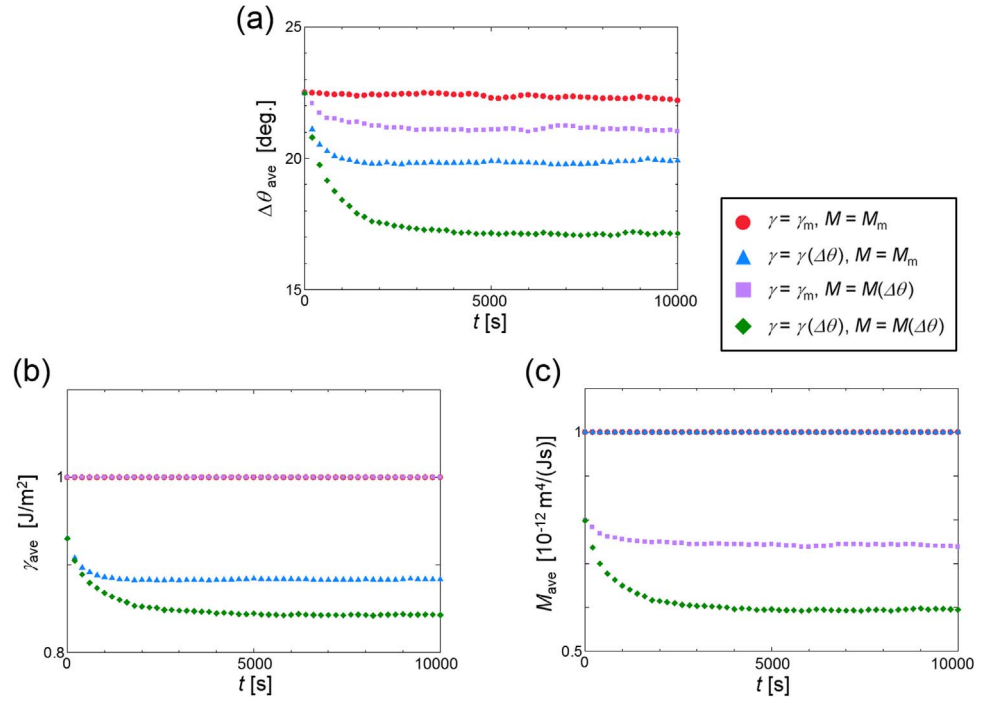

Fig. 4. Temporal variations in (a) $\Delta\theta_{ave}$, (b) γ_{ave}, and (c) M_{ave} obtained under the four different conditions of grain-boundary properties.

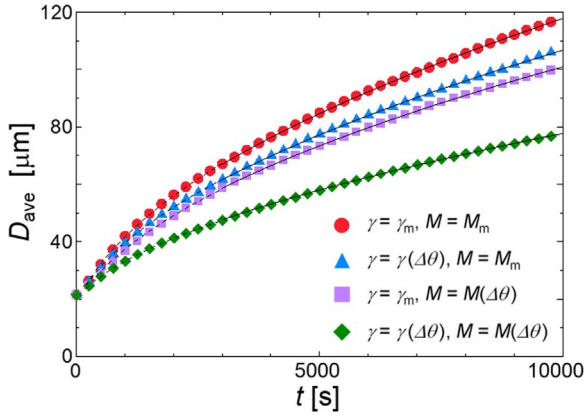

Fig. 5. Temporal variations of D_{ave} obtained for the four different conditions of grain-boundary properties.

Table 1
Grain-growth exponent n extracted for different simulation periods and the four different conditions of grain-boundary properties.

Grain-boundary properties	Grain-growth exponent n	
	200≤ t [s] ≤3000	3000≤ t [s] ≤10,000
$\gamma = \gamma_m$, $M = M_m$	2.00	1.99
$\gamma = \gamma(\Delta\theta)$, $M = M_m$	2.12	2.02
$\gamma = \gamma_m$, $M = M(\Delta\theta)$	2.10	2.04
$\gamma = \gamma(\Delta\theta)$, $M = M(\Delta\theta)$	2.49	2.05

based on two-dimensional grain-growth simulations. The numerical model we employed was a higher-order MPF model capable of representing anisotropic boundary properties with high accuracy. In addition, an effective computing technique using a GPU was utilized to obtain statistically reliable results. Four types of conditions were specified for the grain-boundary properties that were used for each simulation, through which the individual and coupled effects of boundary energy and mobility were tested. The results are summarized as follows:

(1) The anisotropy in both the grain-boundary energy and mobility affects the morphology (the distributions of misorientation angles and grain sizes) formed during grain growth. When they are introduced simultaneously, the evolved morphology displays notable characteristics, in which subgrain-like structures within the high-angle boundary network are clearly observed.
(2) During an initial transient period, the kinetics of anisotropic grain growth deviates from the parabolic growth law, unlike that of isotropic grain growth, subsequent to which the kinetics follows parabolic law. This is because the distribution of the misorientation angles reaches a steady state.

This study examined the fundamental points of anisotropic grain growth by focusing on a two-dimensional system with a random texture. However, it should be emphasized that the dimension, texture, and crystal structure may all affect the nature of anisotropic grain growth. Thus, we plan to study the challenging problem concerning the effects of anisotropic properties in more realistic systems in our future work.

References

[1] G. Gottstein, L.S. Shvindlerman, Grain Boundary Migration in Metals: Thermodynamics, Kinetics, Applications, CRC Press, Boca Raton, 1999.
[2] F.J. Humphreys, M. Hatherly, Recrystallization and Related Annealing Phenomena, second, Pergamon Press, Oxford, 2004.
[3] Y. Shibuta, S. Takamoto, T. Suzuki, ISIJ Int. 48 (2008) 1582.
[4] Y. Shibuta, S. Takamoto, T. Suzuki, Comput. Mater. Sci. 44 (2009) 1025.
[5] J.E. Burke, D. Turnbull, Prog. Met. Phys. 3 (1952) 220.
[6] M. Hillert, Acta Metall. 13 (1965) 227.
[7] N.P. Louat, Acta Metall. 22 (1974) 721.
[8] K. Chang, N. Moelans, Acta Mater. 64 (2014) 443.
[9] H.J. Frost, Y. Hayashi, C.V. Thompson, D.T. Walton, MRS Proc. 338 (2011) 295.
[10] G.S. Grest, D.J. Srolovitz, M.P. Anderson, Acta Metall. 33 (1985) 509.
[11] J. Gruber, H.M. Miller, T.D. Hoffmann, G.S. Rohrer, A.D. Rollett, Acta Mater. 57 (2009) 6102.
[12] E.A. Holm, G.N. Hassold, M.A. Miodownik, Acta Mater. 49 (2001) 2981.
[13] E.A. Holm, M.A. Miodownik, A.D. Rollett, Acta Mater. 51 (2003) 2701.
[14] A. Kazaryan, Y. Wang, S.A. Dregia, B.R. Patton, Acta Mater. 50 (2002) 2491.
[15] J.S. Lee, B.-J. Lee, Y.M. Koo, S.G. Kim, Scr. Mater. 110 (2016) 113.
[16] N. Moelans, F. Spaepen, P. Wollants, Philos. Mag. 90 (2010) 501.
[17] A.D. Rollett, JOM 56 (2004) 63.
[18] A.D. Rollett, D.J. Srolovitz, M.P. Anderson, Acta Metall. 37 (1989) 1227.

[19] Y. Saito, M. Enomoto, ISIJ Int. 32 (1992) 267.
[20] Y. Suwa, Y. Saito, H. Onodera, Comput. Mater. Sci. 40 (2007) 40.
[21] T. Tamaki, K. Murakami, K. Ushioda, Nippon Steel Tech. Rep. 102 (2013) 31.
[22] M. Upmanyu, G.N. Hassold, A. Kazaryan, E.A. Holm, Y. Wang, B. Patton, D.J. Srolovitz, Interface Sci. 10 (2002) 201.
[23] A. Vondrous, M. Reichardt, B. Nestler, Model. Simul. Mater. Sci. Eng. 22 (2014) 025014.
[24] Q. Yu, S.K. Esche, Mater. Lett. 56 (2002) 47.
[25] S.G. Kim, D.I. Kim, W.T. Kim, Y.B. Park, Phys. Rev. E 74 (2006) 061605.
[26] I. Steinbach, F. Pezzolla, B. Nestler, M. Seeßelberg, R. Prieler, G.J. Schmitz, J.L.L. Rezende, Physica D. 94 (1996) 135.
[27] I. Steinbach, F. Pezzolla, Physica D. 134 (1999) 385.
[28] Y. Suwa, Y. Saito, H. Onodera, Comput. Mater. Sci. 44 (2008) 286.
[29] T. Takaki, T. Hirouchi, Y. Hisakuni, A. Yamanaka, Y. Tomita, Mater. Trans. 49 (2008) 2559.
[30] T. Takaki, Y. Tomita, Int. J. Mech. Sci. 52 (2010) 320.
[31] M. Ohno, S. Tsuchiya, K. Matsuura, Acta Mater. 59 (2011) 5700.
[32] J. Gruber, N. Ma, Y. Wang, A.D. Rollett, G.S. Rohrer, Model. Simul. Mater. Sci. Eng. 14 (2006) 1189.
[33] S. Vedantam, B.S.V. Patnaik, Phys. Rev. E 73 (2006) 016703.
[34] H. Garcke, B. Nestler, B. Stoth, SIAM J. Appl. Math. 60 (1999) 295.
[35] B. Nestler, H. Garcke, B. Stinner, Phys. Rev. E 71 (2005).
[36] T. Hirouchi, T. Tsuru, Y. Shibutani, Comput. Mater. Sci. 53 (2012) 474.
[37] E. Miyoshi, T. Takaki, Comput. Mater. Sci. 112 (2016) 44.
[38] T. Takaki, T. Shimokawabe, M. Ohno, A. Yamanaka, T. Aoki, J. Cryst. Growth 382 (2013) 21.
[39] T. Takaki, M. Ohno, T. Shimokawabe, T. Aoki, Acta Mater. 81 (2014) 272.
[40] Y. Shibuta, K. Oguchi, T. Takaki, M. Ohno, Sci. Rep. 5 (2015) 13534.
[41] Y.Shibuta, M.Ohno, T.Takaki, JOM 671793, 2015.
[42] T. Takaki, R. Rojas, M. Ohno, T. Shimokawabe, T. Aoki, IOP Conf. Ser. Mater. Sci. Eng. 84 (2015) 012066.
[43] S. Sakane, T. Takaki, M. Ohno, T. Shimokawabe, IOP Conf. Ser. Mater. Sci. Eng. 84 (2015) 012063.
[44] W.T. Read, W. Shockley, Phys. Rev. 78 (1950) 275.
[45] F.J. Humphreys, Acta Mater. 45 (1997) 4231.